Journal Pre-proof

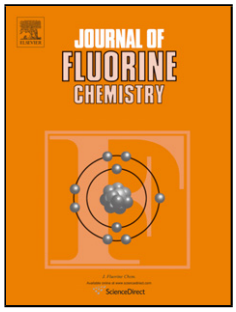

Synthesis, crystal structure and fluorination effects in vinylidenebis(diphenylphosphine)gold(I) thiolate coordination compounds

Guillermo Romo-Islas, Guillermo Moreno-Alcántar, Marcos Flores-Álamo, Hugo Torrens

PII: S0022-1139(20)30276-1

DOI: https://doi.org/10.1016/j.jfluchem.2020.109578

Reference: FLUOR 109578

To appear in: *Journal of Fluorine Chemistry*

Received Date: 28 April 2020

Revised Date: 28 May 2020

Accepted Date: 28 May 2020

Please cite this article as: { doi: https://doi.org/

Synthesis, crystal structure and fluorination effects in vinylidenebis(diphenylphosphine)gold(I) thiolate coordination compounds.

Guillermo Romo-Islas[χ], Guillermo Moreno-Alcántar*[‡], Marcos Flores-Álamo and Hugo Torrens

Facultad de Química, Universidad Nacional Autónoma de México, Circuito Escolar, Ciudad Universitaria, Coyoacán, 04510 Mexico City, Mexico

*Correspondence: lgma@comunidad.unam.mx Tel.: +52 55 5622 3724

Present address:

[χ]Departament de Química Inorgànica i Orgànica, Secció de Química Inorgànica, Universitat de Barcelona, Martí i Franquès 1-11, 08028 Barcelona, Spain

[‡]Institut de Science et d' Ingénierie Supramoléculaires (ISIS), Université de Strasbourg. 8 alleé Gaspard Monge, 67000, Strasbourg, France.

Graphical abstract

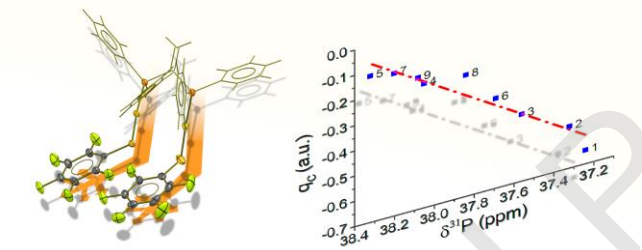

Highlight

- fluorination exerts electronic and supramolecular modifications on gold compounds.
- the *trans*-influence of fluoriation is studied by means of ^{31}P-NMR.
- the different effects of fluor positions can be separated from the NMR influence.

Abstract

We report the synthesis and characterization of nine new gold(I) dinuclear compounds containing the bridging ligand vinylidenebis(diphenylphosphine) and terminal fluorophenylthiolates with the general formula $[Au_2(SR)_2(\mu\text{-vdpp})]$ in which SR = SC_6F_5, SC_6HF_4, $SC_6H_3F_2$-2,4, $SC_6H_3F_2$-3,4, $SC_6H_3F_2$-3,5, SC_6H_4F-2, SC_6H_4F-3, SC_6H_4F-4 together with the non-fluorinated derivative $[Au_2(SC_6H_5)_2(\mu\text{-vdpp})]$. In these compounds, we analyze the long-range influence of the fluorination patterns over the electronic structure in terms of the changes in the ^{31}P-NMR

chemical shifts, showing the different effects depending on the relative fluorination position. Additionally, we present the crystal structure of four of the compounds, showing the presence of supported aurophilic interactions in which the Au···Au distances are modified as a consequence of the lateral interactions formed by the fluorinated phenyl rings. Overall this work gives insights in the effects of ligand fluorination in gold coordination compounds.

Abbreviations

vdpp, vinylidenebis(diphenylphosphine; SR, thiolate group; NMR, Nuclear Magnetic Resonance; ppm, parts per million; DCM, dichloromethane; THT, tetrahydrothiophene; vdW, van der Waals.

Keywords

aurophilic interactions, NMR, thiolate, gold, fluorination effects

1. Introduction

Fluorination is a valuable tool for the tuning of properties of compounds. Particularly, it has been successfully used in the design of drugs and therapeutic agents with all kind of purposes,[1–4] but also there are examples of the use of this tool in the modulation of different properties of organic and inorganic materials, e.g. there is a recent increase in the use of fluorination in the design of optoelectronic materials.[5–7] While the effects of the fluorination in short ranges are well known, their long-range influence is less studied.[8,9] Additionally to the electronic effects that are associated with the inclusion of fluorine in the structure of compounds, the supramolecular interaction patterns associated with fluorinated moieties are another attractive source of modulation, in this case of the supramolecular packing and self-assembly behavior. [6,10,11]

On the other hand, gold(I) coordination compounds have attracted attention in the last decades due to the increasing number of interesting properties of technological relevance such as their luminescent,[12,13] pharmacological[14] and catalytic behavior.[15] In many cases, these interesting properties are promoted or modified by the occurrence of aurophilic (Au···Au) interactions,[16] whose formation is driven by a balance of electronic and supramolecular parameters.[17] The use of fluorinated and unfluorinated thiolate ligands in gold coordination compounds has attracted attention due to their electronic and structural versatility. [18–24]

Being electronic modulation one of the pillars of the fluorine chemistry, herein we have studied the fluorination effects over the properties of gold(I) compounds with phosphines. To this end, we have synthesized and characterized a series of compounds based on 1,1-bis(diphenylphosphane)ethylene (vinylidenebis(diphenylphosphine), vdpp) with the general formula $[Au_2(SR)_2(\mu\text{-vdpp})]$ in which SR = SC_6F_5, **1**; SC_6HF_4, **2**; $SC_6H_3F_2$-2,4, **3**; $SC_6H_3F_2$-3,4, **4**; $SC_6H_3F_2$-3,5, **5**; SC_6H_4F-2, **6**; SC_6H_4F-3, **7**; SC_6H_4F-4, **8** and SC_6H_5, **9**. Our studies show, via the examination of the crystal structures of compounds **1**, **2**, **3** and **8**, the important modulation

which fluorinated moieties can produce over the Au-Au interactions. Moreover, in these compounds, the linear coordination geometry of the gold(I) centers permits the communication between the P and S atoms, allowing us to observe by the shifting of the ^{31}P-NMR signals the electronic influence caused by the fluorinated groups. In fact, the ^{31}P-NMR chemical shift variations are sensitive enough for allowing us to differentiate the long-range effects of fluorination in the diverse positions of the phenylthiolate. Through fitting these effects to an additive model, we separated the contribution of fluorination in the *ortho*, *meta* and *para* positions over the ^{31}P-NMR chemical shift.

2. Results and discussion

2.1. X-ray structures

By the slow diffusion of liquid hexane into a solution of the corresponding compound in CH_2Cl_2, we were able to obtain adequate samples of systems **1**, **2**, **3** and **8** to determine their structures by single-crystal X-ray diffraction. All the compounds display linear coordination geometry around gold atom. While the Au-S bond distances are practically equal in the studied systems, the Au-P distances increase slightly by decreasing the fluorination degree of the thiolate ligand (Table 1). This result evidences the *trans*-influence of the thiolate over the phosphine. Due to the closeness of the P atoms in the structure of the ligand all these compounds show supported Au···Au contacts. There are detectable changes in the aurophilic distances which can be explained by the different arrangements of the thiolate fluorinate rings (Table 1). These arrangements are further discussed for each compound. Overall, the differences are a consequence of the diverse interactions promoted by the fluorination patterns. For instance, in compounds **1** and **2**, the existence of intramolecular π···π and π···S interactions promotes shortened Au···Au distances. Differently, in compounds **2** and **8** the existence of hydrogen atoms in the fluorinated rings promotes the formation of intermolecular H-bonds whose directionality causes the elongation of the Au···Au contact. Altogether, the observed results show that the fluorination is a feasible strategy of modulation of structural properties not only through the important electronic effects but also by the promotion of supramolecular synthons.

Compound 1, [$Au_2(SC_6F_5)_2$(μ-vdpp)]. The molecular structure of compound **1** is shown in Figure 1. The studied crystal corresponds to a monoclinic $P2_{1/c}$ system. The asymmetric unit is constituted by only one molecule of [μ-$Au_2(SC_6F_5)_2$(vdpp)]. The P-Au-S angles are consistent with the Au(I) linear geometry displaying values of 175.46(5)° and 173.14(4)°. The gold atoms present intramolecular aurophilic interactions with Au···Au distances of 3.1857(3) Å. One of the sulfur atoms presents an intramolecular interaction with the adjacent fluorinated phenyl group with a distance S2-centroid of 3.574 Å. This interaction is part of the phenyl rings stacking between the thiolate moieties, which interact with centroid to centroid distances of 4.418 Å. In this compound the Au···Au contact and the stacking interactions act in the same direction, causing the Au···Au distance to be the second shortest among the studied compounds. The adjacent molecules interact forming extended polymeric π···π/π···S stacked structures that grow along the *c* crystallographic axis. The intermolecular distances are 3.874 Å for the $\pi_{centroid}\cdots\pi_{centroid}$ and 3.753 Å for the $\pi_{centroid}$···S1 contact (Figure S1).

Compound 2, [$Au_2(SC_6HF_4)_2$(μ-vdpp)]. Figure 2 shows the crystalline structure of compound **2**. It crystallizes in a monoclinic $P2_{1/c}$ system. In which the asymmetric unit consists of only one molecular entity of [$Au_2(SC_6HF_4)_2$(μ-vdpp)]. Around the gold atoms, a linear coordination geometry is observed whit P-Au-S angles of 174.09(7)° and 175.81(7)°. The supported aurophilic contact displays the shortest distance of the arrangements shown herein, 3.1411(4) Å. Similarly, to compound **1**, the shortening of the Au···Au distance is caused by the existence of intramolecular π-stacking and S···π interactions ($d_{centroids}$ = 3.707 Å and $d_{S\cdots\pi}$ = 3.893 Å) between the thiolate fragments that act in the same direction of Au···Au contacts. While the molecular conformation of compound **2** resembles the observed in compound **1**, the supramolecular crystalline arrangements of both compounds differ importantly. Compound **2** does not show the extended π-stacking network on the crystal. Instead, the molecular units hold together by several H-bonding interactions, promoted by the existence of hydrogen atoms in the fluorinated rings. The most important contacts observed are those of: i) H4···S2, ($d_{H\cdots S}$ = 2.811 Å), ii) the double H10···F6 interaction ($d_{H\cdots F}$ = 2.466 Å) and iii) the H22···F5 contact which is also reciprocal ($d_{H\cdots F}$ = 2.444 Å, Figure 2).

Compound 3, [$Au_2(SC_6H_3F_2$-2,4)$_2$(μ-vdpp)]. The crystalline structure of compound **3** corresponds to the orthorhombic space group P_{bcn}. The analysis of the asymmetric unit shows that it is formed by half a molecule of [$Au_2(SC_6H_3F_2$-2,4)$_2$(μ-vdpp)]. The highly symmetric arrangement of compound **3** presents P-Au-S angles of 176.44(11)° and Au-P and Au-S bond distances of 2.264(3) Å and 2.300(3) respectively. The Au···Au contact in this system is larger than in **1** and **2** (3.2427(8) Å). Once again, the enlargement of this distance seems to be affected by the disposition of the thiolate groups. Differently from **1** and **2**, in compound **3** the fluorinated moieties do not participate into intermolecular stacking interactions, instead, hydrogen bonds, between the fluorine in position 4 of the thiolate and a phosphine hydrogen of the neighboring molecule ($d_{H\cdots F}$ = 2.639 Å), direct the fluorinated rings in opposite directions pulling apart the gold atoms (Figure 3). This conformation is favored also by the formation of intramolecular F···H contacts ($d_{H\cdots F}$ = 2.635 Å) and the existence of an intramolecular π-stacking between the fluorinated ring and a phenyl group on the phosphine ($d_{centroids}$ = 3.947 Å).

Compound 8, [$Au_2(SC_6H_4$F-4$)_2$(μ-vdpp)]. The structure obtained for the crystalline form of **8** (Figure 4) corresponds to a 1:1 solvate of the compound with CH_2Cl_2 which structure belongs to the monoclinic $P2_{1/c}$ space group. The asymmetric unit corresponds to the [$Au_2(SC_6H_4$F-4$)_2$(μ-vdpp)]·CH_2Cl_2 fragment. While the P2-Au2-S2 angle is in agreement with the expected linearity (176.23(8)°) the P1-Au1-S1 moiety is considerably distorted with an angle of 169.53(8)° this deformation evidences the hindrance between the aurophilic interaction and the packing of the thiolate fragment as they act in different directions. Because of this, the Au···Au distance in **8**

results to be the largest observed within the structures addressed herein (3.2597(5) Å). The inclusion of the solvent molecule in the crystalline network seems to play a crucial role in the packing. For instance, $H_{DCM}\cdots S$ and $H_{DCM}\cdots F$ contacts are observed between the compound molecule and the solvent unites. Moreover, several $CH\cdots Cl_{DCM}$ interactions are observed involving both thiolate and phosphine phenyl hydrogens. Thus, the disposition of the thiolate groups in the crystal is determined by these contacts, which preclude an efficient Au···Au interaction.

2.2. Fluorination NMR effects

The fluorination patterns of the thiolate ligands attached to the gold centers modify the electron distribution within the molecule. This modification is communicated to the phosphine ligand through the Au atom and is evidenced by the changes in the ^{31}P-NMR chemical shifts. Such effect, which is related to the *trans*-influence of the thiolate over the phosphine ligand bonded to the gold, has been reported by us with similar trends in related systems.[25,26] The measured ^{31}P chemical shift for the studied compounds are presented in Table 2, a trend related to the fluorination influence is not evidently observed as the chemical shift is not only dependent on the number of fluorine atoms in the phenyl ring but is an outcome of the combined inductive and resonant electronic effects originated by the number and positions of fluorine atoms in the structure. To simplify those two effects the Mulliken electronic population was calculated using as model the isolated gold thiolate moieties.[27] The influence of the fluorination is clearly reflected in the resulting charges. Of particular interest are the charges observed in the carbon bonded to sulfur, sulfur and, gold atoms (Figure 5). The charge variations are pronounced in the carbon, spanning 0.5 a.u., due to the spatial proximity and efficient communication provided by the delocalized π system that exists between this and the fluorine atoms. For the more distant S and Au atoms, the variations occur in a more subtle range (~0.1 a.u.). Surprisingly, the plot of the experimental ^{31}P-NMR values and the calculated charge on the carbon atoms (Figure 5) reveals an interesting correlation. This relation probes the almost undisturbed communication between the fluorinated ring and the phosphorus atom. Furthermore, it shows that the effects of fluorination can be sensed and reported by the ^{31}P-NMR chemical shifts in an unexpected importantly long range.

Additionally, the contribution of the different fluorine atoms attached to the structure can be separated by fitting the observed ^{31}P-NMR chemical shift to a Shoolery-type additive model,[28] the fitting has been done by adjusting the experimental data by minimum square numerical approximation to an additive equation. The obtained model (Equation 1) gives values of calculated ^{31}P-NMR shifts that match the experimental values (Figure 6) with Pearson's R^2 for the prediction of 0.98.

$$\delta^{31}P = 38.08 - 0.44543\ o + 0.09819\ m - 0.14707\ p \qquad \text{Equation 1}$$

In equation 1, 38.08 is the ^{31}P-NMR chemical shift of the parent unflorinated thiobenzene derivative **9** and *o*, *m* and *p* are the entire numbers of fluorine atoms in the *ortho*, *meta* and *para* positions respectively. It can be observed that, congruently with their similar hyperconjugation

effects, *ortho* and *para* fluorination exert an upfield shift of the ^{31}P resonance while the mostly inductive effect of the fluorination in *meta* acts in the opposite direction with a considerably smaller contribution.

Conclusions

By the analysis of this family of compounds we have shown the relevance of fluorination to modulate the electronic properties of compounds, in particular, we pointed out the surprisingly long-range influence that fluorine has over distant atoms which are big enough to be followed and analyzed in terms of NMR. Additionally, we show the potential of fluorination as a useful tool to exert supramolecular modulation by promoting the rise of different interaction synthons that can act concomitantly or against other interactions, as shown in this case with aurophilic contacts.

Experimental

Reagents. tetrahydrothiophene (THT), $H[AuCl_4]$, vdpp and all the thiols were purchased from Sigma-Aldrich and used as received. [AuCl(THT)],[29] and lead thiolates[11] were prepared according to reported procedures. $[Au_2Cl_2(\mu\text{-vdpp})]$[30] was prepared by a modification of the reported method detailed in the SI.[31]

General method for the preparation of $[Au_2(SR)_2(\mu\text{-vdpp})]$. In a round bottom flask, a solution of the precursor $[Au_2Cl_2(\mu\text{-vdpp})]$ 100.0 mg (0.116 mmol) in 10 mL of CH_2Cl_2 was mixed under stirring at room temperature with a solution (or suspension for most of the less fluorinated and less soluble lead thiolates) of 0. 0.116 mmol of $Pb(SR_F)_2$ in 10 mL of acetone. After three hours of stirring the mixture was filtrated to eliminate the formed $PbCl_2$ and a clear solution was obtained. The solvent was later evaporated until a volume of about 3 mL and then 20 mL of hexane were added to promote the precipitation of the product in the pure product. The obtained powder was filtrated and washed with hexane (3x 15 mL).

Compound 1, $[Au_2(SC_6F_5)_2(\mu\text{-vdpp})]$: White powder, 92 % yield, mp 227-230°C, IR; v 3054 (=*CH₂*), 1478 (*CH₂)*, 1080 (*C-F*). ^1H NMR (600.17 MHz, $CDCl_3$): δ 6.28 (m, 2 H), 7.47 (m, 8 H) 7.56 (m, 12 H). ^{19}F NMR (564.73 MHz, $CDCl_3$): δ -132.21 (d, J=26.76 Hz, 4 F), -163.13 (t, J=20.09 Hz, 2 F), -164.45 (t, J=23.63 Hz, 4 F). ^{31}P NMR (242.95 MHz, $CDCl_3$): δ 37.24 ppm. APCI (GC-MS) *m/z* : 989 [M-SR_F], 1524 [M+AuSR_F], 2121 [2M-Au], 2316 [2M] Analysis Calculated to $C_{38}H_{22}Au_2F_{10}P_2S_2$ C, 38.40; H, 1.87; S, 5.39 Found C, 38.45; H, 1.85; S, 5.24.

Compound 2, $[Au_2(SC_6HF_4)_2(\mu\text{-vdpp})]$: White powder, 91 % yield, mp 190-192°C, IR; v 3055 (=*CH₂*), 2899 (*ar)*, 1475 (*CH₂)*, 1100 (*C-F*). ^1H NMR (600.17 MHz, $CDCl_3$): δ 6.28 (m, 2 H), 6.63 (tt, J= 9.71, 7.17 Hz, 2 H), 7.45 (m, 8 H), 7.52 (t, J=7.11 Hz, 4H), 7.60 (q, J= 7.03, 6.93 Hz, 8 H). ^{19}F NMR (564.73 MHz, $CDCl_3$): δ -132.54 (m, 4 F), -141.4 (m, 4F). ^{31}P NMR (242.95 MHz, $CDCl_3$): δ 37.32 ppm. APCI (GC-MS) *m/z* : 986 [M-SR_F], 1337 [M+Au], 1714 [M+Au+ AuSR_F]. Analysis Calculated to $C_{38}H_{24}Au_2F_8P_2S_2$ C, 39.60; H, 2.10; S, 5.56 Found C, 39.52; H, 2.02; S, 5.56.

Compound 3, $[Au_2(SC_6H_3F_2\text{-}2,4)_2(\mu\text{-vdpp})]$: White powder, 89 % yield, mp 204-206°C, IR; v 3051 (=*CH₂*), 2953 (*ar)*, 1477 (*CH₂)*, 1081 (*C-F*). ^1H NMR (600.17 MHz, $CDCl_3$): δ 6.24 (m, 2 H), 6.60 (dt,

J=9.77, 4.69 Hz, 2 H), 6.67 (td, J= 9.02, 8.99, 2.82 Hz,2 H), 7.43 (t, J=7.54 Hz, 8 H), 7.51 (dt, J= 14.4, 7.57 Hz, 6 H), 7.57 (q, J= 6.97, 6.90 Hz, 8 H). ^{19}F NMR (564.73 MHz, $CDCl_3$): δ -100.71 (s (br), 2 F), -117.20 (s (br), 2 F). ^{31}P NMR (242.95 MHz, $CDCl_3$): δ 37.56 ppm. APCI (GC-MS) *m/z* : 933 [M-SR_F], 1082 [M], 1277 [M+Au], 1422 [M+AuSR_F]. Analysis Calculated to $C_{38}H_{28}Au_2F_4P_2S_2$ C, 42.24; H, 2.61; S, 5.93 Found C, 42.14; H, 2.58; S, 5.88.

Compound 4, [Au_2($SC_6H_3F_2$-3,4)$_2$(μ-vdpp)]: White powder, 87 % yield, mp 187-189°C, IR; v 3057 (=*CH_2*), 2990 (*ar)*, 1480 (*CH_2)*, 1102 (*C-F*). ^{1}H NMR (600.17 MHz, $CDCl_3$): δ 6.28 (m, 2 H), 6.78 (dt, J=10.56, 8.56 Hz, 2 H), 7.11 (m, 4 H), 7.45 (m, 8 H), 7.56 (m, 12 H). ^{19}F NMR (564.73 MHz, $CDCl_3$): δ -139.03 (m, 2 F), -145.85 (s (br), 2 F). ^{31}P NMR (242.95 MHz, $CDCl_3$): δ 38.05 ppm. APCI (GC-MS) *m/z* : 932 [M-SR_F], 1082 [M], 1422 [M+AuSR_F]. Analysis Calculated to $C_{38}H_{28}Au_2F_4P_2S_2$ C, 42.24; H, 2.61; S, 5.93 Found C, 42.14; H, 2.58; S, 5.88.

Compound 5, [Au_2($SC_6H_3F_2$-3,5)$_2$(μ-vdpp)]: White powder, 92 % yield, mp 152-154°C, IR; v 3054 (=*CH_2*), 1435 (*CH_2)*, 1084 (*C-F*). ^{1}H NMR (600.17 MHz, $CDCl_3$): δ 6.30 (m, 2 H), 6.38 (tt, J=9.12, 2.29 Hz, 2 H), 6.89 (m, 4 H), 7.46 (m, 8 H), 7.54 (t, J= 7.47 Hz, 4 H), 7.59 (m, 8 H). ^{19}F NMR (564.73 MHz, $CDCl_3$): δ -112.35 (s (br), 2 F). ^{31}P NMR (242.95 MHz, $CDCl_3$): δ 38.30 ppm. APCI (GC-MS) *m/z* : 930 [M-SR_F], 1082 [M], 1277 [M+Au], 1422 [M+AuSR_F]. Analysis Calculated to $C_{38}H_{28}Au_2F_4P_2S_2$ C, 42.24; H, 2.61; S, 5.93 Found C, 42.14; H, 2.58; S, 5.88.

Compound 6, [Au_2(SC_6H_4F-2)$_2$(μ-vdpp)]: White powder, 86 % yield, mp 85-87°C, IR; v 3052 (=*CH_2*), 2866 (*ar)*, 1435 (*CH_2)*, 1099 (*C-F*). ^{1}H NMR (600.17 MHz, $CDCl_3$): δ 6.25 (m, 2 H), 6.86 (m, 2 H), 6.91 (m, 6 H), 7.43 (t, J=7.57 Hz, 8 H), 7.53 (t, J=7.42 Hz, 4 H), 7.60 (dt, J=7.84, 4.64 Hz, 8 H). ^{19}F NMR (564.73 MHz, $CDCl_3$): δ -105.51 (s (br), 2 F). ^{31}P NMR (242.95 MHz, $CDCl_3$): δ 37.69 ppm. APCI (GC-MS) *m/z* : 917 [M-SR_F], 1044 [M], 1241 [M+Au]. Analysis Calculated to $C_{38}H_{22}Au_2F_{10}P_2S_2$ C, 43.69; H, 2.89; S, 6.14 Found C, 43.55; H, 2.80; S, 5.89.

Compound 7, [Au_2(SC_6H_4F-3)$_2$(μ-vdpp)]: White powder, 88 % yield, mp 120-122°C, IR; v 3056 (=*CH_2*), 2870 (*ar)*, 1463 (*CH_2)*, 1099 (*C-F*). ^{1}H NMR (600.17 MHz, $CDCl_3$): δ 6.27 (m, 2 H), 6.63 (td, J= 8.38, 8.37, 2.51 Hz, 2 H), 6.95 (td, J= 7.97, 7.84, 6.29 Hz, 2 H), 7.08 (d, J=10.15 Hz, 2 H), 7.22 (d, J=7.92 Hz, 2 H), 7.43 (tt, J=7.34, 1.54 Hz, 8 H), 7.52 (m, 4 H), 7.60 (m, 8H). ^{19}F NMR (564.73 MHz, $CDCl_3$): δ -114.73 (s (br), 2 F). ^{31}P NMR (242.95 MHz, $CDCl_3$): δ 38.20 ppm. APCI (GC-MS) *m/z* : 918 [M-SR_F], 1044 [M], 1241 [M+Au], 1583 [M+Au+Au SR_F]. Analysis Calculated to $C_{38}H_{22}Au_2F_{10}P_2S_2$ C, 43.69; H, 2.89; S, 6.14 Found C, 43.55; H, 2.80; S, 5.89.

Compound 8, [Au_2(SC_6H_4F-4)$_2$(μ-vdpp)]: White powder, 86 % yield, mp 138-140°C, IR; v 3053 (=*CH_2*), 2870 (*ar)*, 1463 (*CH_2)*, 1099 (*C-F*). ^{1}H NMR (600.17 MHz, $CDCl_3$): δ 6.26 (m, 2 H), 6.71 (tt, J= 8.38, 9.54, 2.12 Hz, 4 H), 7.35 (m, 4 H), 7.43 (t, J=7.52 Hz, 8 H), 7.53 (d, J=7.22 Hz, 4 H), 7.57 (m, 8 H). ^{19}F NMR (564.73 MHz, $CDCl_3$): δ -121.17 (s (br), 2 F). ^{31}P NMR (242.95 MHz, $CDCl_3$): δ 37.84 ppm. APCI (GC-MS) *m/z* : 918 [M-SR_F], 1044 [M], 1241 [M+Au], 1583 [M+Au+Au SR_F]. Analysis Calculated to $C_{38}H_{22}Au_2F_{10}P_2S_2$ C, 43.69; H, 2.89; S, 6.14 Found C, 43.55; H, 2.80; S, 5.89.

Compound 9, [Au_2(SC_6H_5)$_2$(μ-vdpp)]: White powder, 85 % yield, mp 78-80°C, IR; v 305 (=*CH_2*), 2868 (*ar)*, 1434 (*CH_2)*, 1098 (*C-F*). ^{1}H NMR (600.17 MHz, $CDCl_3$): δ 6.26 (m, 2 H), 6.94 (t, J= 7.30 Hz, 2 H)

7.02 (t, J= 7.51 Hz, 4 H), 7.41 (t, J= 7.52 Hz, 8 H), 7.45 (d, J= 7.64 Hz, 4 H), 7.51 (t, J= 7.47 Hz, 4 H), 7.60 (q, J= 6.92, 6.72 Hz, 8 H). ^{31}P NMR (242.95 MHz, $CDCl_3$): δ 38.08 ppm. APCI (GC-MS) *m/z* : 899 [M-SR_F], 1008 [M], 1312 [M+$AuSR_F$], 1511 [M+Au+Au SR_F]. Analysis Calculated to $C_{38}H_{32}Au_2F_{10}P_2S_2$ C, 45.25; H, 3.20; S, 6.36 Found C, 45.20; H, 3.13; S, 6.31.

Crystal Structure Determination

Suitable single crystals of compounds **1**, **2**, **3** and **8** were mounted on glass fibers and crystallographic data were collected with an Oxford Diffraction Gemini "A" diffractometer with a CCD area detector with monochromator of graphite for $\lambda_{MoK\alpha}$ = 0.71073 Å. CrysAlisPro and CrysAlis RED software packages were used for data collection and integration.[32] The double-pass method of scanning was used to exclude any noise. The collected frames were integrated by using an orientation matrix determined from the narrow frame scans. Final cell constants were determined by a global refinement; collected data were corrected for absorbance by using analytical numeric absorption correction using a multifaceted crystal model based on expressions upon the Laue symmetry with equivalent reflections.[33] Structures solutions and refinement were carried out with the SHELXS-2014 [34] and SHELXL-2014[35] packages. WinGX v2018.3[36] software was used to prepare material for publication. Full-matrix least-squares refinement was carried out by minimizing $(Fo^2 - Fc^2)^2$. All non-hydrogen atoms were refined anisotropically. H atoms attached to C atoms were placed in geometrically idealized positions and refined as riding on their parent atoms, with C–H = 0.95–0.97 Å and with U_{iso}(H) = 1.2U_{eq}(C) for aromatic and methylene groups. On the other hand, for compound **2**, the solvent molecules were significantly disordered and could not be modeled properly, thus SQUEEZE, a part of the PLATON[37] package of crystallographic software, was used to calculate the solvents disorder areas and remove their contributions to the overall intensity data, The disordered solvents area is centered around the 0.00 0.50 1.00 position and showing an estimated total of 76 electrons and a void volume of 222 Å^3. C1, C2, C3, C4 ,C5, C6, F1 ,F2 and C1P, C2P, C3P ,C4P ,C5P, C6P, F1P ,F2P are disordered over two sites with occupancies 0.47:0.53 in **3.** Crystallographic data for all complexes is presented in Table 2. The crystallographic data for the structures reported in this paper have been deposited with the Cambridge Crystallographic Data Centre as supplementary publication no. CCDC 1999611-1999614. Copies of the data can be obtained free of charge on application to CCDC, 12 Union Road, Cambridge, CB2 1EZ, UK (fax: (+44) 1223-336-033, e-mail: deposit@ccdc.cam.ac.uk).

Declaration of interests

The authors declare that they have no known competing financial interests or personal relationships that could have appeared to influence the work reported in this paper.

Acknowledgments

We acknowledge the financial support from DGAPA-UNAM project IN210818 and CONACYT-Mexico CB-2012/177498 along with the postdoctoral grant 740732 for G.M.A., G.R.I.

acknowledges the scholarship from Fundación Carolina-SRE and the support of Prof. Laura Rodríguez. We also thank Unit for Support to Research and Industry (USAII) of the Faculty of Chemistry – UNAM for the instrumental Support.

References

[1] H. Mei, J. Han, S. Fustero, M. Medio-Simon, D.M. Sedgwick, C. Santi, R. Ruzziconi, V.A. Soloshonok, Fluorine-Containing Drugs Approved by the FDA in 2018, Chem. - A Eur. J. (2019). https://doi.org/10.1002/chem.201901840.

[2] C. Au, C. Gonzalez, Y.C. Leung, F. Mansour, J. Trinh, Z. Wang, X.G. Hu, R. Griffith, E. Pasquier, L. Hunter, Tuning the properties of a cyclic RGD-containing tetrapeptide through backbone fluorination, Org. Biomol. Chem. 17 (2019) 664–674. https://doi.org/10.1039/c8ob02679c.

[3] N.A. Meanwell, Fluorine and Fluorinated Motifs in the Design and Application of Bioisosteres for Drug Design, J. Med. Chem. 61 (2018) 5822–5880. https://doi.org/10.1021/acs.jmedchem.7b01788.

[4] Z. Zhang, W. Shen, J. Ling, Y. Yan, J. Hu, Y. Cheng, The fluorination effect of fluoroamphiphiles in cytosolic protein delivery, Nat. Commun. 9 (2018). https://doi.org/10.1038/s41467-018-03779-8.

[5] K. Weng, X. Xue, F. Qi, Y. Zhang, L. Huo, J. Zhang, D. Wei, M. Wan, Y. Sun, Synergistic Effects of Fluorination and Alkylthiolation on the Photovoltaic Performance of the Poly(benzodithiophene-benzothiadiazole) Copolymers, ACS Appl. Energy Mater. 1 (2018) 4686–4694. https://doi.org/10.1021/acsaem.8b00819.

[6] M. Spengler, R.Y. Dong, C.A. Michal, M. Pfletscher, M. Giese, Fluorination of supramolecular liquid crystals-tuning tool and analytical probe, J. Mater. Chem. C. 5 (2017) 2235–2239. https://doi.org/10.1039/c6tc05472b.

[7] N.V.S.D.K. Bhupathiraju, W. Rizvi, J.D. Batteas, C.M. Drain, Fluorinated porphyrinoids as efficient platforms for new photonic materials, sensors, and therapeutics, Org. Biomol. Chem. 14 (2016) 389–408. https://doi.org/10.1039/c5ob01839k.

[8] E. Silva-Nigenda, A. Martínez-Gómez, J. Cruz-de la Cruz, J. Barroso-Flores, C. González-Romero, A. Fuentes-Benites, C.K. Jankowski, E. Cuevas-Yáñez, E. Díaz-Torres, D. Corona-Becerril, Long range $^{1}H–^{19}F$ coupling through multiple bond in thienopyridines, isoquinolines and 2-aza-carbazoles derivatives, J. Mol. Struct. 1176 (2019) 562–566. https://doi.org/10.1016/j.molstruc.2018.08.084.

[9] J. Gräfenstein, D. Cremer, Unusual long-range spin-spin coupling in fluorinated polyenes: A mechanistic analysis, J. Chem. Phys. 127 (2007). https://doi.org/10.1063/1.2787001.

[10] V.R. Thalladi, H.-C. Weiss, D. Bläser, R. Boese, A. Nangia, G.R. Desiraju, C–H···F Interactions in the Crystal Structures of Some Fluorobenzenes, J. Am. Chem. Soc. 120 (1998) 8702–

8710. https://doi.org/10.1021/ja981198e.

[11] G. Moreno-Alcántar, L. Salazar, G. Romo-Islas, M. Flores-Álamo, H. Torrens, Exploring the Self-Assembled Tacticity in Aurophilic Polymeric Arrangements of Diphosphanegold(I) Fluorothiolates, Molecules. 24 (2019) 4422. https://doi.org/10.3390/molecules24234422.

[12] X. He, V.W.-W. Yam, Luminescent gold(I) complexes for chemosensing, Coord. Chem. Rev. 255 (2011) 2111–2123. https://doi.org/10.1016/j.ccr.2011.02.003.

[13] E.E. Langdon-Jones, S.J.A. Pope, Recent developments in gold(<scp>i</scp>) coordination chemistry: luminescence properties and bioimaging opportunities, Chem. Commun. 50 (2014) 10343. https://doi.org/10.1039/C4CC03259D.

[14] T. Zou, C.T. Lum, C.-N. Lok, J.-J. Zhang, C.-M. Che, Chemical biology of anticancer gold(III) and gold(I) complexes, Chem. Soc. Rev. 44 (2015) 8786–8801. https://doi.org/10.1039/C5CS00132C.

[15] A.M. Echavarren, A.S.K. Hashmi, F.D. Toste, Gold Catalysis - Steadily Increasing in Importance, Adv. Synth. Catal. 358 (2016) 1347–1347. https://doi.org/10.1002/adsc.201600381.

[16] H. Schmidbaur, A. Schier, A briefing on aurophilicity, Chem. Soc. Rev. 37 (2008) 1931. https://doi.org/10.1039/b708845k.

[17] G. Moreno-Alcántar, G. Romo-Islas, M. Flores-Álamo, H. Torrens, Aurophilicity vs. thiophilicity: directing the crystalline supramolecular arrangement in luminescent gold compounds, New J. Chem. 42 (2018) 7845–7852. https://doi.org/10.1039/C7NJ04354F.

[18] B.-C. Tzeng, A. Schier, H. Schmidbaur, Crystal Engineering of Gold(I) Thiolate Based Compounds via Cooperative Aurophilic and Hydrogen-Bonding Interactions, Inorg. Chem. 38 (1999) 3978–3984. https://doi.org/10.1021/ic990308v.

[19] E.R.T. Tiekink, J.-G. Kang, Luminescence properties of phosphinegold(I) halides and thiolates, Coord. Chem. Rev. 253 (2009) 1627–1648. https://doi.org/10.1016/j.ccr.2009.01.017.

[20] M. Bardají, M.J. Calhorda, P.J. Costa, P.G. Jones, A. Laguna, M. Reyes Pérez, M.D. Villacampa, Synthesis, Structural Characterization, and Theoretical Studies of Gold(I) and Gold(I)−Gold(III) Thiolate Complexes: Quenching of Gold(I) Thiolate Luminescence, Inorg. Chem. 45 (2006) 1059–1068. https://doi.org/10.1021/ic051168u.

[21] S. Montanel-Pérez, A. Izaga, A. Laguna, M.D. Villacampa, M.C. Gimeno, Synthesis of Gold(III) Complexes with Bidentate Amino-Thiolate Ligands as Precursors of Novel Bifunctional Acyclic Diaminocarbenes, ACS Omega. 3 (2018) 13097–13103. https://doi.org/10.1021/acsomega.8b01547.

[22] R. Visbal, R.P. Herrera, M.C. Gimeno, Thiolate Bridged Gold(I)–NHC Catalysts: New Approach for Catalyst Design and its Application to Trapping Catalytic Intermediates, Chem. – A Eur. J. 25 (2019) 15837–15845. https://doi.org/10.1002/chem.201903494.

[23] V.W.W. Yam, C.-L.L. Chan, C.-K.K. Li, K.M.C. Wong, V. Wing-Wah Yam, C.-L.L. Chan, C.-K.K. Li, K. Man-Chung Wong, Molecular design of luminescent dinuclear gold(I) thiolate complexes: from fundamentals to chemosensing, Coord. Chem. Rev. 216217 (2001) 173–194. https://doi.org/10.1016/S0010-8545(01)00310-1.

[24] S.Y. Ho, E.C.-C. Cheng, E.R.T. Tiekink, V.W.-W. Yam, Luminescent Phosphine Gold(I) Thiolates: Correlation between Crystal Structure and Photoluminescent Properties in [R_3PAu{SC(OMe)$NC_6H_4NO_2$-4}] (R = Et, Cy, Ph) and [(Ph_2P-R-PPh_2){AuSC(OMe)$NC_6H_4NO_2$-4}2] (R = CH_2, $(CH_2)_2$, $(CH_2)_3$, $(CH_2)_4$, Fc), Inorg. Chem. 45 (2006) 8165–8174. https://doi.org/10.1021/ic0608243.

[25] G. Moreno-Alcántar, H. Hernández-Toledo, J.M. Guevara-Vela, T. Rocha-Rinza, Á. Martín Pendás, M. Flores-Álamo, H. Torrens, Stability and trans Influence in Fluorinated Gold(I) Coordination Compounds, Eur. J. Inorg. Chem. 2018 (2018) 4413–4420. https://doi.org/10.1002/ejic.201800567.

[26] G. Moreno-Alcántar, K. Hess, J.M. Guevara-Vela, T. Rocha-Rinza, Á. Martín Pendás, M. Flores-Álamo, H. Torrens, π-Backbonding and non-covalent interactions in the JohnPhos and polyfluorothiolate complexes of gold(I), Dalton Trans. 46 (2017) 12456–12465. https://doi.org/10.1039/C7DT00961E.

[27] M.J. Frisch, G.W. Trucks, H.B. Schlegel, G.E. Scuseria, M.A. Robb, J.R. Cheeseman, G. Scalmani, V. Barone, B. Mennucci, G.A. Petersson, H. Nakatsuji, M. Caricato, X. Li, H.P. Hratchian, A.F. Izmaylov, J. Bloino, G. Zheng, J.L. Sonnenberg, M. Hada, M. Ehara, K. Toyota, R. Fukuda, J. Hasegawa, M. Ishida, T. Nakajima, Y. Honda, O. Kitao, H. Nakai, T. Vreven, J.A. Montgomery Jr., J.E. Peralta, F. Ogliaro, M. Bearpark, J.J. Heyd, E. Brothers, K.N. Kudin, V.N. Staroverov, R. Kobayashi, J. Normand, K. Raghavachari, A. Rendell, J.C. Burant, S.S. Iyengar, J. Tomasi, M. Cossi, N. Rega, J.M. Millam, M. Klene, J.E. Knox, J.B. Cross, V. Bakken, C. Adamo, J. Jaramillo, R. Gomperts, R.E. Stratmann, O. Yazyev, A.J. Austin, R. Cammi, C. Pomelli, J.W. Ochterski, R.L. Martin, K. Morokuma, V.G. Zakrzewski, G.A. Voth, P. Salvador, J.J. Dannenberg, S. Dapprich, A.D. Daniels, Ö. Farkas, J.B. Foresman, J. V Ortiz, J. Cioslowski, D.J. Fox, Gaussian 09, Revision D.01, Gaussian Inc. (2009). https://doi.org/10.1159/000348293.

[28] J.N. Shoolery, Technical Information Bulletin, Varian Associates, Palo Alto, USA, 1959.

[29] E.A. Allen, W. Wilkinson, The vibrational spectra of some dialkyl sulphide complexes of gold(III) and gold(I) halides, Spectrochim. Acta Part A Mol. Spectrosc. 28 (1972) 2257–2262. https://doi.org/10.1016/0584-8539(72)80200-9.

[30] H. Schmidbaur, R. Herr, G. Mueller, J. Riede, Activation of vinylidenebis(diphenylphosphine) through metal complexation, Organometallics. 4 (1985) 1208–1213. https://doi.org/10.1021/om00126a013.

[31] P. Braunstein, T.M.G. Carneiro, D. Matt, F. Balegroune, D. Grandjean, β-Keto phosphines derived from ferrocene. Syntheses and structures of [$Ph_2PCH_2C(O)(\eta^5$-$C_5H_4)Fe(\eta^5$-$C_5H_5)$] (L1) and trans-[$PdCl_2L1_2$], J. Organomet. Chem. 367 (1989) 117–132.

https://doi.org/10.1016/0022-328X(89)87213-4.

[32] Agilent, CrysAlis PRO, (2014).

[33] R.C. Clark, J.S. Reid, The analytical calculation of absorption in multifaceted crystals, Acta Crystallogr. Sect. A Found. Crystallogr. 51 (1995) 887–897. https://doi.org/10.1107/S0108767395007367.

[34] G.M. Sheldrick, SHELXT – Integrated space-group and crystal-structure determination, Acta Crystallogr. Sect. A Found. Adv. 71 (2015) 3–8. https://doi.org/10.1107/S2053273314026370.

[35] G.M. Sheldrick, Crystal structure refinement with SHELXL, Acta Crystallogr. Sect. C Struct. Chem. 71 (2015) 3–8. https://doi.org/10.1107/S2053229614024218.

[36] L.J. Farrugia, WinGX and ORTEP for Windows: An update, J. Appl. Crystallogr. 45 (2012) 849–854. https://doi.org/10.1107/S0021889812029111.

[37] A.L. Spek, PLATON SQUEEZE: A tool for the calculation of the disordered solvent contribution to the calculated structure factors, Acta Crystallogr. Sect. C Struct. Chem. 71 (2015) 9–18. https://doi.org/10.1107/S2053229614024929.

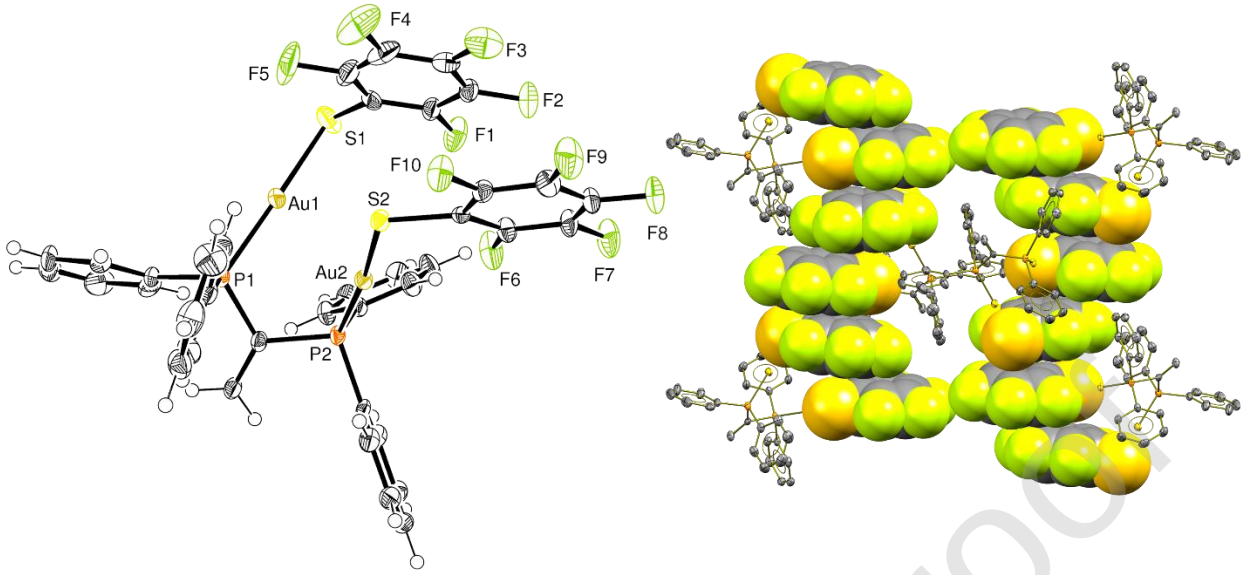

*Figure 1. Left: Molecular structure of compound **1** with displacement ellipsoids at 50% probability level for non-H atoms. Right: Extended π-stacked/S···π structures formed in the crystalline packing of **1**, the spheres radii equals the van der Waals radii of the elements and the ellipsoids are shown at 50% probability level, H atoms were omitted for clarity. Selected distances (Å): Au1-Au2, 3.1857(3); P2-Au2, 2.2574(13); P1-Au1, 2.2539(12); Au2-S2, 2.3061(13); Au1-S1, 2.2970(13). Selected angles (°) P1-C25-P2,112.6(2); P1-Au1-S1, 175.46(5); P2-Au2-S2, 173.14(4); Au1-S1-C1, 103.09(15); Au2-S2-C7, 109.80(16).*

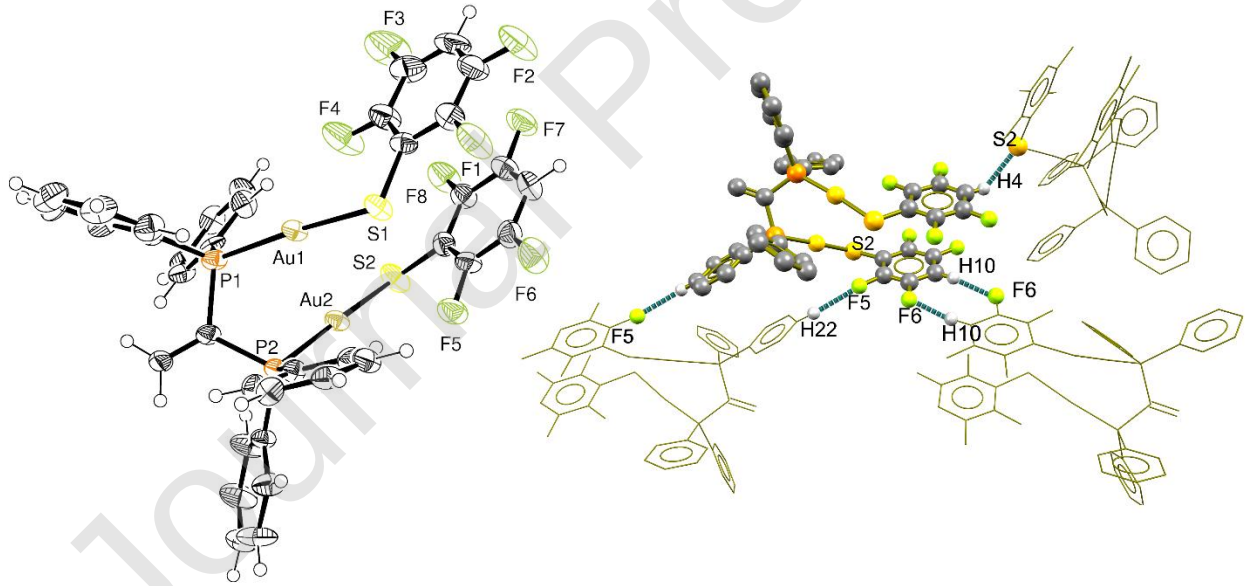

*Figure 2. Left: Crystal structure of compound **2,** the displacement ellipsoids are presented at 50% probability level for non-H atoms. Right: Short intermolecular H-bond interactions ($d_{H\text{-}A}$ < sum of vdW radii - 0.1) around a molecule in the packing of compound **2**. Selected distances (Å): Au1-Au2, 3.1411(4); P2-Au2, 2.2551(19); P1-Au1, 2.2568(19); Au2-S2, 2.296(2); Au1-S1, 2.2974(19). Selected angles (°) P1-C25-P2,112.4(4); P1-Au1-S1, 174.09(7); P2-Au2-S2, 175.81(7); Au1-S1-C1, 110.6(3); Au2-S2-C7, 108.4(3).*

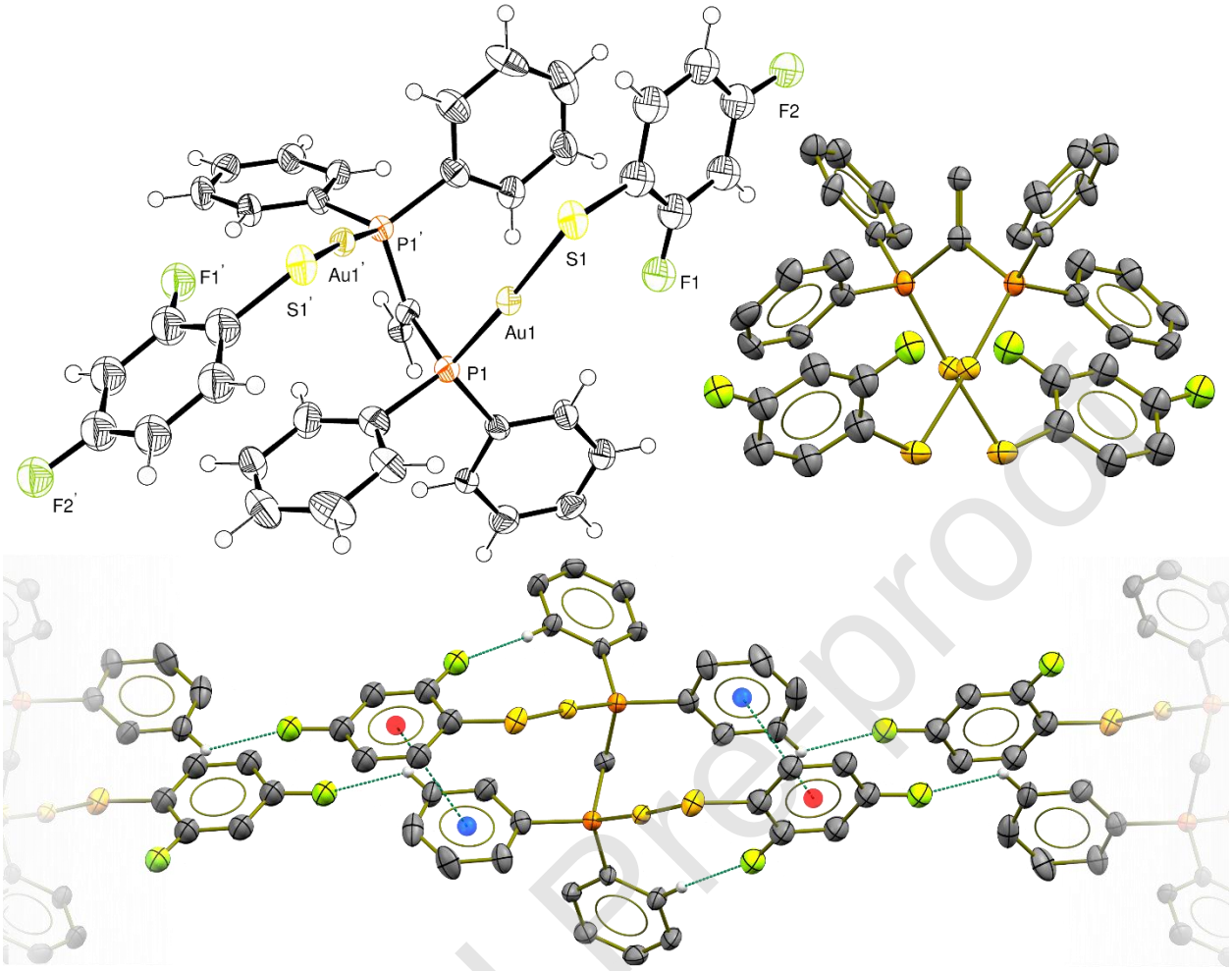

*Figure 3. Top left: View in perspective of the structure of compound **3** with displacement ellipsoids at 50% probability level for non-H atoms. Top right: view of the molecule along the Au···Au contact showing the symmetric disposition of the thiolate groups. Bottom: non-covalent interactions between neighboring molecules of **3**. Selected distances (Å): Au1-Au1, 3.2427(8); P1-Au1, 2.264(3); Au1-S1, 2.300(3). Selected angles (°) P1-C25-P1,113.5(9); P1-Au1-S1, 176.44(11); Au1-S1-C1, 105.5(9).*

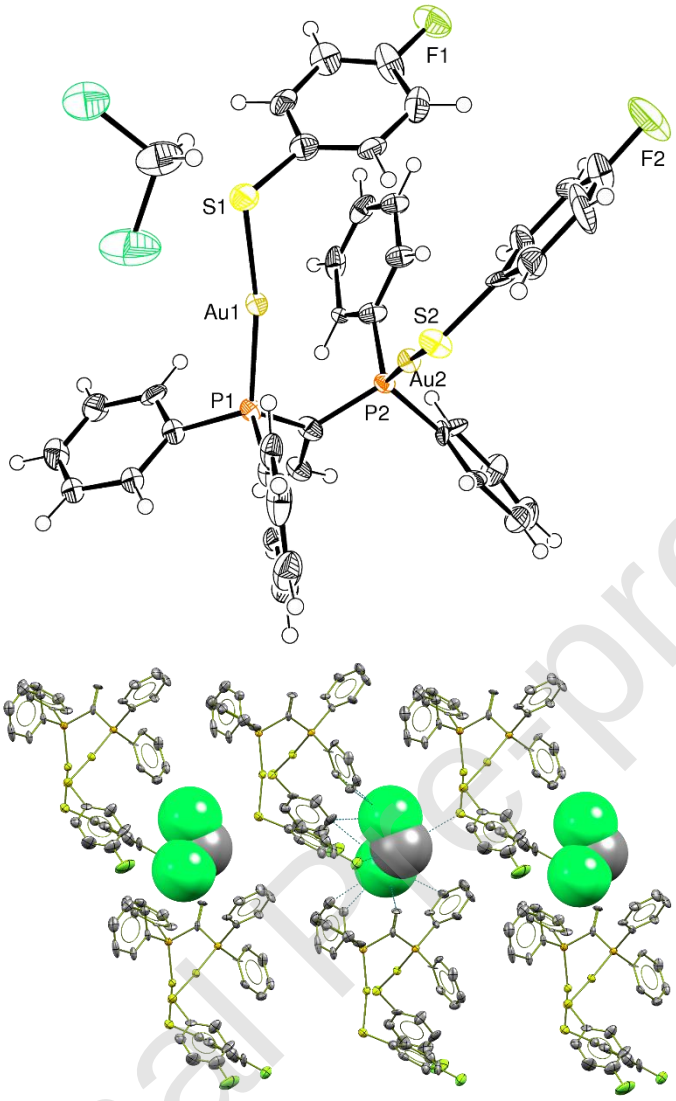

*Figure 4. Top: Molecular structure of compound **8**·CH_2Cl_2 with displacement ellipsoids at 50% probability level for non-H atoms. Bottom: Solid-state packing of **8**·CH_2Cl_2 highlighting the position of the solvent molecules, the spheres radii equals the van der Waals radii of the elements and the ellipsoids are shown at 50% probability level, H atoms were omitted for clarity. Selected distances (Å): Au1-Au2, 3.2597(5); P2-Au2, 2.263(2); P1-Au1, 2.268(2); Au2-S2, 2.300(2); Au1-S1, 2.297(3). Selected angles (°) P1-C25-P2,111.9(5); P1-Au1-S1, 169.53(8); P2-Au2-S2, 176.23(8); Au1-S1-C1, 107.0(3); Au2-S2-C7, 108.6(3).*

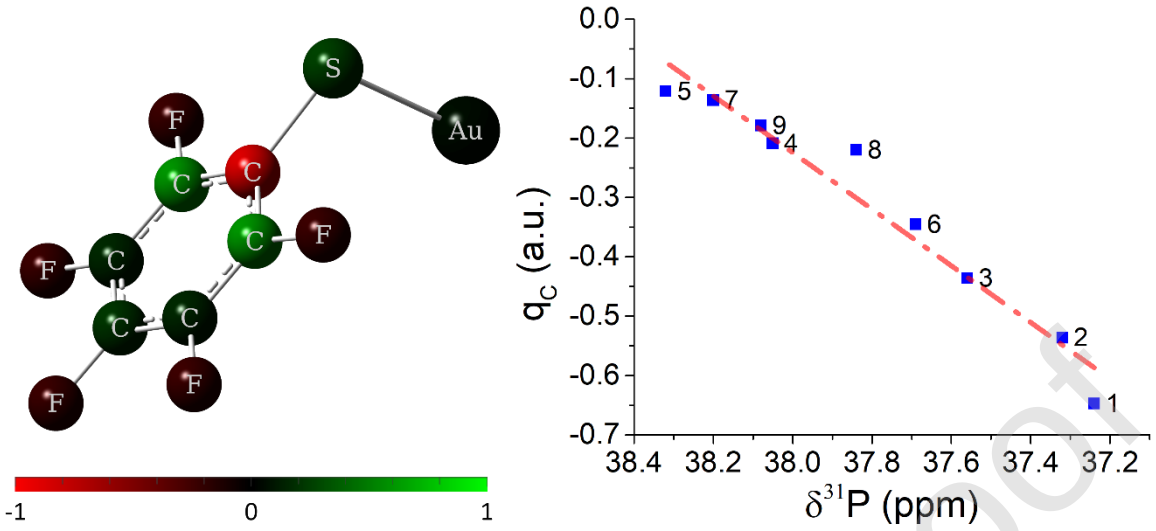

*Figure 5 Left: Calculated Mulliken charge distribution in the model system $AuSC_6F_5$ as reported in Table 1, each atom's color indicates the value of its charge in a.u. according to the scale shown below. Right: Plot showing the correlation between the calculated Mulliken charge of the sulfur's base carbon atom for model systems **1**-**9**.*

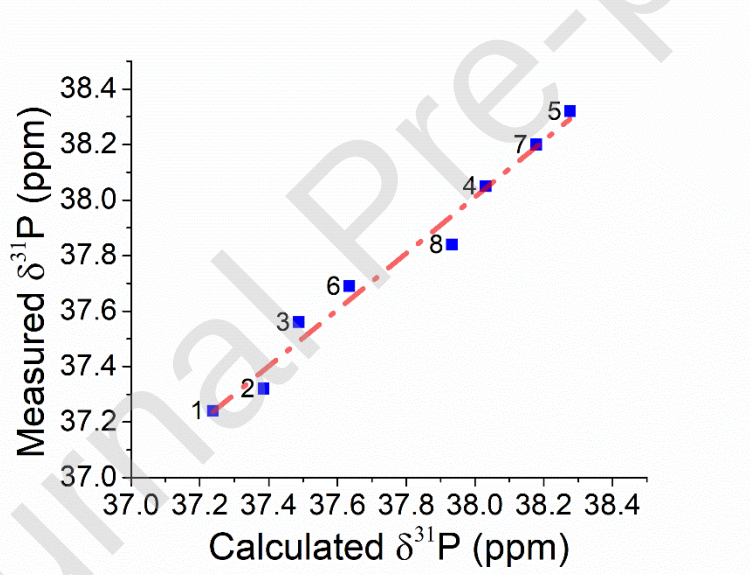

Figure 6 Goodness of the estimation of the ^{31}P NMR chemical shift values by Equation 1.

*Table 1. Selected intramolecular distances in the structures determined by X-ray of compounds **1**, **2**, **3** and **8**.*

Compound	d_{Au-Au} (Å)	d_{Au-P} (Å)		d_{Au-S} (Å)		$d_{\pi-\pi}$ (Å)	$d_{\pi-S}$ (Å)
1	3.1857(3)	2.254(1)	2.257(1)	2.297(1)	2.306(1)	3.874	3.753
2	3.1411(4)	2.255(2)	2.256(2)	2.296(2)	2.297(2)	3.707	3.893
3	3.2427(8)	2.264(3)	-	2.300(3)	-	3.947	-
8	3.2597(5)	2.268(2)	2.263(2)	2.297(3)	2.300(2)	-	-

Table 2. ^{31}P Chemical shifts and calculated Mulliken population of the atoms of Au, S and C_S in the free gold thiolate.

Compound	δ ^{31}P (ppm)	q_{Au} (a.u.)	q_S (a.u.)	q_{C*} (a.u.)
1	37.24	0.048	0.197	-0.647
2	37.32	0.043	0.170	-0.536
3	37.56	0.019	0.136	-0.436
4	38.05	0.006	0.123	-0.209
5	38.32	0.017	0.120	-0.121
6	37.69	-0.009	0.098	-0.345
7	38.20	-0.021	0.085	-0.136
8	37.84	-0.033	0.089	-0.220
9	38.08	-0.044	0.078	-0.179

*Carbon atom directly bonded to sulfur

.

*Table 2. Crystal data and structure refinement for **1**, **2**, **3** and **8**.*

Compound (Identification code)	**1** (VdppAuF5-720)	**2** (vdpauf4h-613_sq)	**3** (vauf224-117)	**8** (vdppauf4-001)
Empirical formula	$C_{38}H_{22}Au_2F_{10}P_2S_2$	$C_{38}H_{24}Au_2F_8P_2S_2$	$C_{38}H_{28}Au_2F_4P_2S_2$	$C_{39}H_{30}Au_2Cl_2F_2P_2S_2$
Formula weight	1188.55	1152.56	1080.60	1127.52
Temperature	130(2) K	130(2) K	130(2) K	130(2) K
Wavelength	0.71073 Å	0.71073 Å	0.71073 Å	0.71073 Å
Crystal system	Monoclinic	Monoclinic	Orthorhombic	Monoclinic
Space group	P 21/c	P 21/c	P b c n	P 21/n
Unit cell dimensions	a = 13.271(3) Å b = 21.9104(17) Å c = 14.057(2) Å β= 115.81(2)°.	a = 12.4959(7) Å b = 14.8424(7) Å c = 21.2449(11) Å β= 89.917(5)°.	a = 10.1120(4) Å b = 15.4180(6) Å c = 22.2416(13) Å	a = 13.0402(8) Å b = 14.9871(7) Å c = 19.6055(9) Å β= 100.523(5)°.
Volume	3679.6(12) $Å^3$	3940.3(4) $Å^3$	3467.6(3) $Å^3$	3767.2(3) $Å^3$
Z	4	4	4	4
Density (calculated)	2.145 Mg/m^3	1.943 Mg/m^3	2.070 Mg/m^3	1.988 Mg/m^3
Absorption coefficient	8.245 mm^{-1}	7.690 mm^{-1}	8.714 mm^{-1}	8.156 mm^{-1}
F(000)	2240	2176	2048	2144
Crystal size	0.490 x 0.270 x 0.110 mm^3	0.370 x 0.170 x 0.060 mm^3	0.440 x 0.340 x 0.060 mm^3	0.250 x 0.220 x 0.040 mm^3
Theta range for data collection	3.457 to 29.613°.	3.538 to 29.644°.	3.447 to 29.532°.	3.413 to 29.639°.
Index ranges	-14<=h<=17, -26<=k<=30, -17<=l<=18	-17<=h<=17, -20<=k<=20, -29<=l<=28	-12<=h<=13, -18<=k<=20, -30<=l<=20	-15<=h<=18, -20<=k<=16, -26<=l<=26
Reflections collected	19086	43916	11519	21777
Independent reflections	8654 [R(int) = 0.0375]	9905 [R(int) = 0.0670]	4154 [R(int) = 0.0652]	8936 [R(int) = 0.0701]
Completeness to theta = 25.242°	99.7 %	99.7 %	99.7 %	99.8 %
Absorption correction	Analytical	Analytical	Analytical	Analytical
Max. and min. transmission	0.508 and 0.153	0.619 and 0.185	0.572 and 0.112	0.741 and 0.229
Refinement method	Full-matrix least-squares on F^2	Full-matrix least-squares on F^2	Full-matrix least-squares on F^2	Full-matrix least-squares on F^2
Data / restraints / parameters	8654 / 0 / 487	9905 / 0 / 469	4154 / 0 / 177	8936 / 30 / 412
Goodness-of-fit on F^2	1.029	1.035	1.032	1.045
Final R indices [I>2sigma(I)]	R1 = 0.0324, wR2 = 0.0498	R1 = 0.0437, wR2 = 0.0804	R1 = 0.0596, wR2 = 0.1385	R1 = 0.0544, wR2 = 0.0981
R indices (all data)	R1 = 0.0526, wR2 = 0.0566	R1 = 0.0956, wR2 = 0.1015	R1 = 0.0942, wR2 = 0.1723	R1 = 0.0973, wR2 = 0.1202
Largest diff. peak and hole	0.888 and -1.167 $e.Å^{-3}$	2.814 and -1.207 $e.Å^{-3}$	2.961 and -2.514 $e.Å^{-3}$	3.213 and -1.407 $e.Å^{-3}$